Chapter 3
Experimental Cremation of Bone: Crystallite Size and Lattice Parameter Evolution

Martina Greiner, Balazs Kocsis, Mario F. Heinig, Katrin Mayer, Anita Toncala, Gisela Grupe, and Wolfgang W. Schmahl

Abstract In this study we investigate pristine and experimentally incinerated bovine bone material with differing annealing times and temperatures from 100 to 1000 °C to analyse the crystallographic change of natural bone mineral during cremation. We used X-ray powder diffraction (XRPD) and Fourier transform infrared (FTIR) spectroscopy as complementary methods. We observe a structural change of bone mineral during cremation. Our study highlights that there are only few or even no hydroxyl ions in pristine bone mineral (bioapatite), which is a carbonate-hydroapatite rather than a hydroxyapatite. A significant recrystallization reaction from bioapatite to hydroxyapatite takes place at elevated temperatures from 700 °C (after 30 min cremation time). This process is associated with a significant increase of crystallite size, and it involves an increase of hydroxyl in the apatite lattice that goes along with a depletion of water and carbonate contents during cremation. Our first results highlight the importance of both time and temperature on the recrystallization reaction during cremation.

Keywords Carbonated apatite · Calcium phosphate · Bioapatite · Bone · X-ray diffraction · FTIR · Rietveld refinement

M. Greiner (✉) · B. Kocsis · M. F. Heinig · W. W. Schmahl
Department für Geo- und Umweltwissenschaften, Ludwig-Maximilians-Universität, Munich, Germany
e-mail: martina.greiner@lrz.uni-muenchen.de; wolfgang.schmahl@lrz.uni-muenchen.de

K. Mayer · A. Toncala · G. Grupe
Fakultät für Biologie, Anthropologie und Humangenetik, Ludwig-Maximilians-Universität, Martinsried, Germany
e-mail: katrin.mayer@mnet-online.de; G.Grupe@lrz.uni-muenchen.de

K. Endo et al. (eds.), *Biomineralization*,
https://doi.org/10.1007/978-981-13-1002-7_3

3.1 Introduction

The Forschergruppe FOR 1670 project on human transalpine mobility in the Late Bronze Age to Early Roman times performs isotope studies on archaeological bone finds. During that age, cremating the deceased was the primary burial custom (Grupe et al. 2015). To understand bone alteration by cremation, we study the evolution of bone crystallography and crystallite size as a function of cremation temperature and annealing time for bovine bone by FTIR and X-ray diffraction. Mammal bone mineral is a nanocrystalline material consisting of an apatite mineral that is chemically far more complex than hydroxyapatite and can be approximated as $(Ca,Mg,Na)_{10-x}((PO_4)_{6-x}(CO_3)_x)(OH_{1-y-z}, (CO_3)_y, (H_2O)_z)_2$ (Elliott 2002; Rey et al. 2007). It comprises between 5 and 8 wt% carbonate, which substitutes in the $[OH]^-$ site (A-type substitution) as well as the $[PO]_4^{3-}$ site (B-type substitution) of the apatite structure (LeGeros et al. 1969; Wopenka and Pasteris 2005; Pasteris et al. 2012; Yi et al. 2013). Previous studies showed that recrystallization of the bioapatite and crystallite growth mainly sets in from about 600 °C (Piga et al. 2009; Schmahl et al. 2017), but small changes are already apparent at low temperatures of 100 °C (Harbeck et al. 2011). In this study, we want to define more precisely the cremation temperature and annealing time where hydroxyapatite crystallization sets in.

3.2 Materials and Methods

Pieces of compact bone were cut from the tubular part of bovine femur; the endosteal and periosteal surfaces were mechanically removed. Samples were ultrasonically washed in deionized H_2O. After air-drying, the bones were defatted for 5 days with diethyl ether in a Soxhlet and air-dried. Finally, the samples were homogenized to a fine powder and passed through a 100 µm sieve.

Cremation experiments were carried out between 100 and 1000 °C in air (oxidizing conditions) in steps of 100 °C with 150 min annealing time. After data analysis of the initial results, we focussed on the temperatures of 650 and 700 °C and used shorter exposure times between 10 and 60 min in intervals of 10 min.

X-ray diffractograms were collected on a General Electric 3003 powder diffractometer in Bragg-Brentano reflection geometry. Cu-$K_{\alpha 1}$ radiation was selected with an exposure time of 1000s.

All samples were mixed with NIST 660b LaB_6 as internal standard (2–5 wt%). The FULLPROF code (Rodríguez-Carvajal 1993; Rodríguez-Carvajal and Roisnel 2004) was applied for data evaluation and Rietveld refinement (Rietveld 1969). The Thompson-Cox-Hastings method for convolution of instrumental resolution with size and isotropic microstrain broadening (Thompson et al. 1987) was applied. For refinement, a hexagonal symmetry model for carbonated apatite was used (Wilson et al. 2004).

Infrared spectra were measured on a Bruker Equinox FTIR instrument with a resolution of 4 cm^{-1} with 128 scans.

3.3 Results

3.3.1 X-Ray Diffraction: 100 °C Intervals

Figure 3.1a shows X-ray powder diffraction patterns of untreated and cremated bones up to 1000 °C. The untreated bone mineral displays extremely broadened peaks. The broadening decreases only little with 150 min heat treatment up until 600 °C, whereas the diffraction pattern sharpens considerably from 700 °C upwards.

Exemplary Rietveld refinements of samples cremated at 600 °C and 700 °C for 150 min annealing time are shown in Fig. 3.1b, c. Enlarged images of the 31–35° 2θ section show overlapping apatite diffraction peaks in Fig. 3.1b, whereas peaks in Fig. 3.1c can clearly be distinguished from each other. The lattice parameters and crystallite sizes obtained by Rietveld refinement of diffractograms measured at room temperature for the 150 min heat-treated samples are shown in Fig. 3.1d, e. Note the sharp rise of the crystallite size setting in at 700 °C. The lattice parameters show an initial increase with annealing treatment and then sharply drop at temperatures where the grain size sharply increases.

3.3.2 X-Ray Diffraction: 10 Min Intervals

The X-ray diffractograms of the bovine bone cremated at 650 °C from 10 to 60 min depict a steady narrowing of the diffraction peaks with increasing annealing time. Nevertheless, a broad peak shape remains after 60 min annealing (Fig. 3.2a). The unit cell parameters shrink (Fig. 3.2b, c) already after 20 min cremation. The crystallite size increases more or less steadily with elapsed annealing time, whereas the biggest change is between 30 and 40 min with an increase of the crystallite size of 99.4(2) Å to 126.6(3) Å (Fig. 3.2c).

X-ray diffractograms of bovine bone cremated at 700 °C from 10 to 60 min show a broad diffraction peak shape from 10 to 30 min annealing time. Samples annealed for 40 min or longer depict sharper peaks. Bovine bone incinerated at 700 °C shows a steady increase of the crystallite size up to 30 min experimental cremation. From 30 to 40 min elapsing time, we observe a significant jump from 117.85(2) Å to 294.8(3) Å (2.5 times larger) (Fig. 3.2f). Moreover, we observe a decrease of lattice parameters a and c until 40 min annealing times. This trend is reversed after 50 min annealing (Fig. 3.2e, f).

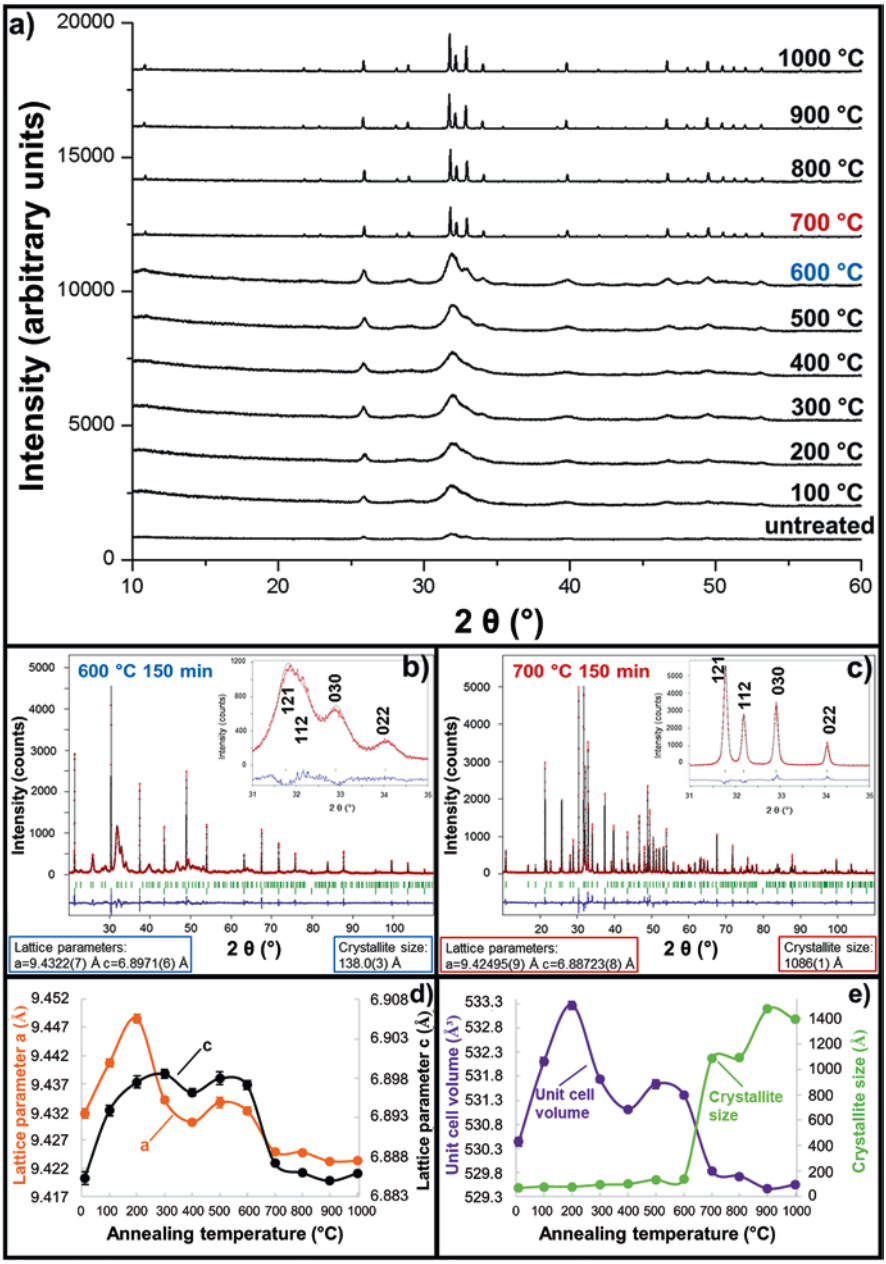

Fig. 3.1 (**a**) Comparison of the 10–60° 2θ range of X-ray diffractograms (Cu-$K_{\alpha 1}$) of cremated bones from 100 to 1000 °C; (**b**) Rietveld refinement of bovine bone cremated at 600 °C, 150 min annealing. *Red dots*, observed data points; *black line*, calculated XRD profile; *bottom blue line*, difference of observed and calculated data; *green vertical bars*, positions of diffraction peaks; *top row*, bone apatite; *bottom row*, LaB_6 standard. Enlarged region shows 31–35° 2θ range with overlapping 121, 112, 030 and 022 peaks; (**c**) Rietveld refinement of bovine bone cremated at 700 °C after 150 min annealing. Enlarged region shows 30–35° 2θ range with clearly distinct 121, 112, 030 and 022 peaks; (**d**) Lattice parameters a (=b) and c of untreated and annealed bone material at temperatures from 100 to 1000 °C after 150 min annealing; (**e**) Unit cell volume and crystallite size of untreated and cremated bones from 100 to 1000 °C after 150 min annealing

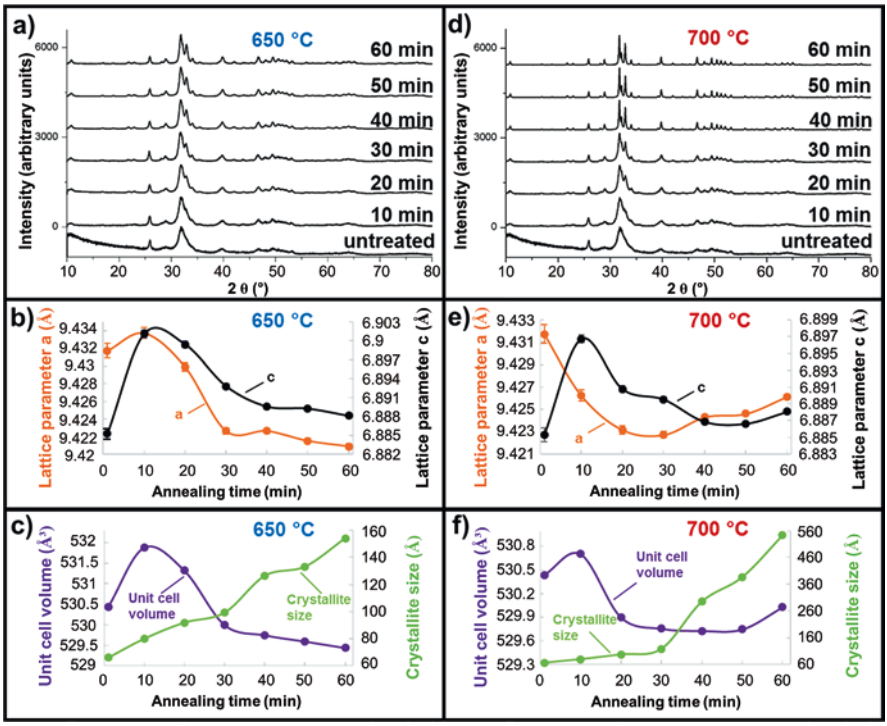

Fig. 3.2 (**a**) Comparison of the 10–80° 2θ range of X-ray diffractograms (Cu-$K_{\alpha 1}$) of untreated and cremated bones at 650 °C, 10–60 min annealing; (**b**) Lattice parameters a (=b) and c of untreated and cremated bones at 650 °C, 10–60 min annealing; (**c**) Unit cell volume and crystallite size of untreated and cremated bones at 650 °C, 10–60 min annealing; (**d**) 10–80° 2θ range of X-ray diffractograms of untreated and cremated bones at 700 °C, 10–60 min annealing; (**e**) Lattice parameters a(=b) and c of untreated and cremated bones at 700 °C, 10–60 min annealing; (**f**) Unit cell volume and crystallite size of untreated and cremated bones at 700 °C, 10–60 min annealing

3.3.3 FTIR

Figure 3.3a shows a comparison of IR spectra for different annealing temperatures. Characteristic phosphate group absorption bands at 470–480 cm^{-1} ($\nu_2PO_4^{3-}$), 500–750 cm^{-1} ($\nu_4PO_4^{3-}$), ~962 cm^{-1} ($\nu_1PO_4^{3-}$) and 980–1120 cm^{-1} ($\nu_3PO_4^{3-}$) were identified according to Destainville et al. (2003) and Raynaud et al. (2002). Annealed bone at 1000 °C shows a well-differentiated hydroxyl libration peak at ~632 cm^{-1} which is absent in the FTIR spectra of untreated bovine bone (Fig. 3.3b).

Absorption bands at 873–879 cm^{-1} and 1400–1458 cm^{-1} were attributed to $\nu_2CO_3^{2-}$ and $\nu_3CO_3^{2-}$ (Fleet 2009; Grunenwald et al. 2014; Rey et al. 1989). The intensity of carbonate bands begins to decrease from 400 °C with increasing annealing temperatures and can barely be observed for the sample cremated at 1000 °C (see Fig. 3.3a). For untreated bovine bone, we observe broad H_2O absorption bands from ~3000 to 3600 cm^{-1} (Brubach et al. 2005). These peaks lose intensity with heat treatment and disappear for the 700 °C and higher heat treatments (Fig. 3.3c).

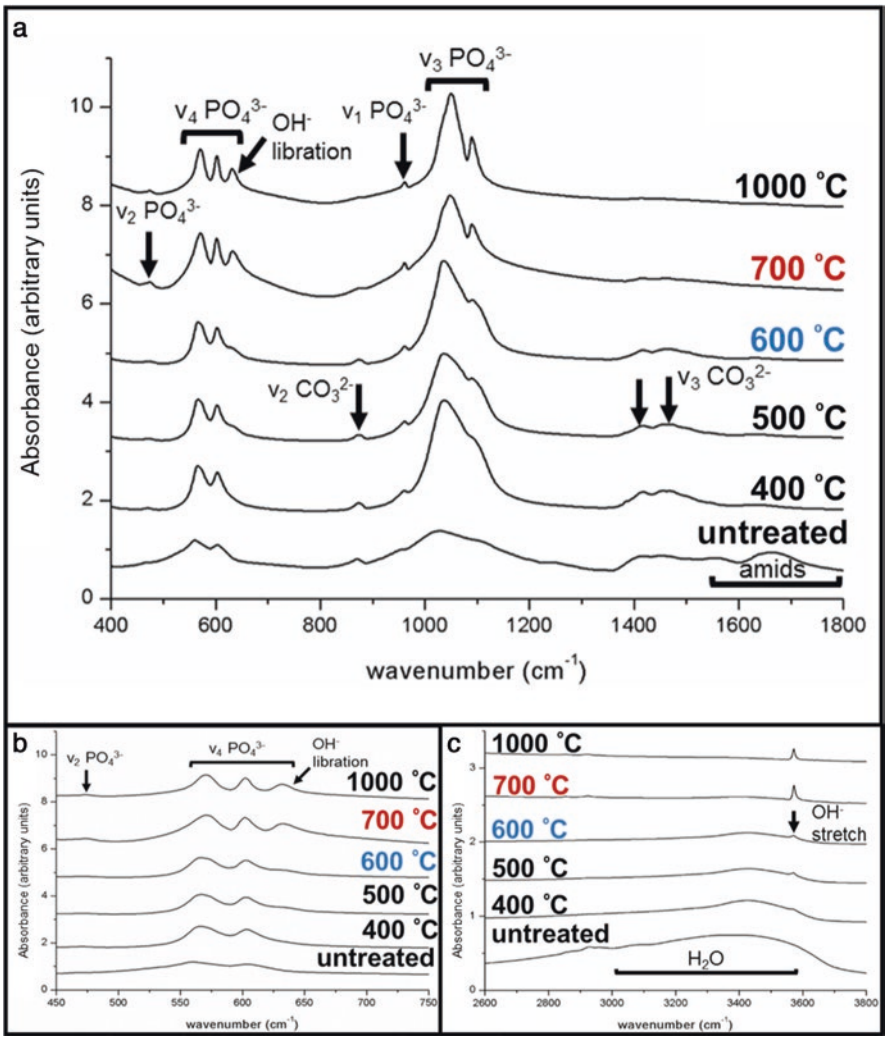

Fig. 3.3 (**a**) Comparison of the 400–1800 cm^{-1} FTIR spectra of untreated and cremated bovine bone at 400, 500, 600, 700 and 1000 °C (annealing time 150 min); (**b**) Enlargement of the 450–750 cm^{-1} region of Fig. 3.2a) with $\nu_2PO_4^{3-}$ and $\nu_4PO_4^{3-}$ vibration bands and emerging OH^- libration band with increasing cremation temperature; (**c**) 2600–3800 cm^{-1} region of untreated and cremated bone (400, 500, 600, 700 and 1000 °C) indicating decreasing H_2O absorption bands and increasing OH^- stretching mode with increasing cremation temperature

The OH^- stretch vibration gives a sharp peak at 3570 cm^{-1} (González-Díaz and Hidalgo 1976; González-Díaz and Santos 1977; Vandecandelaere et al. 2012). The band at ~632 cm^{-1} was assigned to the OH^- libration mode (Destainville et al. 2003). In the untreated bone spectra and for low annealing temperatures, neither the OH^- libration peak near 630 cm^{-1} nor the sharp and distinct OH^- stretching vibration

peak at 3570 cm^{-1} is present. However, these OH^- signals emerge with annealing at 400 °C and significantly increase and become well-differentiated for samples annealed at temperatures of 700 °C or higher (see Fig. 3.3b, c).

3.4 Discussion

In the original bone, we observe broad diffraction peaks (Figs. 3.1a and 3.2a, b) due to the nanoscale dimension of the bone apatite crystallites. Further, the high intensity of the carbonate and H_2O vibration bands and absence of OH^- bands quite clearly indicate that bone apatite is a carbonate-hydro-apatite rather than a hydroxyapatite (Fig. 3.3a–c). Loong et al. (2000) using inelastic neutron scattering and Pasteris et al. (2004) using Raman spectroscopy came to similar conclusions.

With extended annealing treatment, the diffraction peaks of the bone mineral get sharper; the $(CO_3)^{2-}$ infrared signals decrease, while the OH^- infrared peaks increase. Within the broad water band, one can clearly see the rising of the OH^- stretching is a function of increasing annealing temperature (Fig. 3.3c). This indicates a reaction from bioapatite (carbonate-hydro-apatite) to hydroxyapatite with heat treatment, as the material approaches stoichiometric chemistry. This reaction is associated with growth of the crystallites; the growth becomes more rapid at temperatures from 700 °C and higher (Figs. 3.1a and 3.2d). At the same time, loss of carbonate and water and their replacement by OH^- in the structure lead to a decrease of unit cell parameters (Figs. 3.1d, e and 3.2b–f).

While observing these structural changes occurring, it cannot be simply concluded that the process occurs homogeneously within the apatite lattice. It is just as likely that the bioapatite decomposes and that hydroxyapatite is formed in a heterogeneous reaction at the expense of the decomposing bioapatite. It must be borne in mind that our techniques integrate over the whole volume of the sample, and the diffraction peak positions as well as IR frequencies of both mineral phases (bioapatite and hydroxyapatite) are very close and initially severely broadened. Thus our techniques might well record a superposition of the signals of both phases coexisting. Here it is important to note that the distinct increase of the crystallite size for temperatures of and above 700 °C sets in after 30 min of annealing time (Fig. 3.2e, f). This may be indicative of a heterogeneous rather than a homogeneous reaction from bioapatite to hydroxyapatite. For an increase of crystallite size of only one homogeneous apatite phase by Ostwald ripening, the evolution of crystallite size with time (Fig. 3.2f) should have the opposite curvature than observed.

The time dependence (Fig. 3.2) of the reaction process becomes important when concluding from bone crystallinity to cremation temperature. Up to 40 min cremation time, we see the same trend for lattice parameters when comparing 650 and 700 °C: a decrease of lattice parameters a and c and therefore a shrinkage of the unit cell coupled with an increase of the crystallite size (Fig. 3.2b–f). After more than 30 min annealing at 700 °C, we see more rapidly increasing lattice parameters, an effect which is not observable in the 650 °C temperature experiments. Moreover, at

700 °C after 30 min annealing, we observe also a significant change in crystallite size which we attribute to a progressive recrystallization reaction of bioapatite to hydroxyapatite. At that time, the decomposition products (essentially carbon) of organics such as collagen, which comprise about 35 wt% of the original bone material (Rogers and Zioupos 1999), are almost completely gone, and the hydroxyapatite crystallites can grow without being impeded by films of organics or their residues which separate the crystallites.

Note that bone annealed at 400 °C for 150 min displays essentially the same crystallite sizes as bone treated for 20 min at 700 °C (~97 Å), and bone annealed at 600 °C for 150 min displays similar crystallite sizes as bone treated at 650 °C for 50 min (~133 Å). Our experiments reveal that it is important to consider the influence of time when concluding from material state on cremation conditions.

Acknowledgement We thank the Deutsche Forschungsgemeinschaft (DFG) for funding the project in Forschergruppe FOR1670 under Schm930/12-1 and Gr 959/20-1,2.

References

Brubach JB et al (2005) Signatures of the hydrogen bonding in the infrared bands of water. J Chem Phys 122:184509

Destainville A et al (2003) Synthesis, characterization and thermal behavior of apatitic tricalcium phosphate. Mater Chem Phys 80:269–277

Elliott JC (2002) Calcium phosphate biominerals. Rev Mineral Geochem 48:427–453

Fleet ME (2009) Infrared spectra of carbonate apatites: v2-region bands. Biomaterials 30:1473–1481

González-Díaz PF, Hidalgo A (1976) Infrared spectra of calcium apatites. Spectrochim Acta A 32:631–635

González-Díaz PF, Santos M (1977) On the hydroxyl ions in apatites. J Solid State Chem 22:193–199

Grunenwald A et al (2014) Revisiting carbonate quantification in apatite (bio)minerals: a validated FTIR methodology. J Archaeol Sci 49:134–141

Grupe G et al (2015) Prähistorische Anthropologie. Springer, Berlin

Harbeck M et al (2011) Research potential and limitations of trace analyses of cremated remains. Forensic Sci Int 204:191–200

LeGeros RZ et al (1969) Two types of carbonate substitution in the apatite structure. Experientia 25:5–7

Loong CK et al (2000) Evidence of hydroxyl-ion deficiency in bone apatites: an inelastic neutron-scattering study. Bone 26:599–602

Pasteris JD et al (2004) Lack of OH in nanocrystalline apatite as a function of degree of atomic order: implications for bone and biomaterials. Biomaterials 25:229–238

Pasteris JD et al (2012) Effect of carbonate incorporation on the hydroxyl content of hydroxylapatite. Mineral Mag 76:2741–2759

Piga G et al (2009) The potential of X-ray diffraction in the analysis of burned remains from forensic contexts. J Forensic Sci 54:534–539

Raynaud S et al (2002) Calcium phosphate apatites with variable Ca/P atomic ratio I. Synthesis, characterisation and thermal stability of powders. Biomaterials 23:1065–1072

Rey C et al (1989) The carbonate environment in bone mineral: a resolution-enhanced Fourier Transform Infrared Spectroscopy study. Calcif Tissue Int 45:157–164

Rey C et al (2007) Physico-chemical properties of nanocrystalline apatites: implications for biominerals and biomaterials. Mater Sci Eng C 27:198–205
Rietveld HM (1969) A profile refinement method for nuclear and magnetic structures. J Appl Crystallogr 2:65–71
Rodríguez-Carvajal J (1993) Recent advances in magnetic structure determination by neutron powder diffraction. Physica B 192:55–69
Rodríguez-Carvajal J, Roisnel T (2004) Line broadening analysis using FullProf*: determination of microstructural properties. Mater Sci Forum 443–444:123–126
Rogers KD, Zioupos P (1999) The bone tissue of the rostrum of a *Mesoplodon densirostris* whale: a mammalian biomineral demonstrating extreme texture. J Mater Sci Lett 18:651–654
Schmahl WW et al (2017) The crystalline state of archaeological bone material. In: Across the Alps in prehistory. Springer International Publishing, Cham
Thompson P, Cox DE, Hastings JB (1987) Rietveld refinement of Debye–Scherrer synchrotron X-ray data from Al_2O_3. J Appl Crystallogr 20:79–83
Vandecandelaere N et al (2012) Biomimetic apatite-based biomaterials: on the critical impact of synthesis and post-synthesis parameters. J Mater Sci Mater Med 23:2593–2606
Wilson RM et al (2004) Rietveld structure refinement of precipitated carbonate apatite using neutron diffraction data. Biomaterials 25:2205–2213
Wopenka B, Pasteris JD (2005) A mineralogical perspective on the apatite in bone. Mater Sci Eng C 25:131–143
Yi H et al (2013) A carbonate-fluoride defect model for carbonate-rich fluorapatite. Am Mineral 98:1066–1069